Future Technology
Open Access Journal
ISSN 2832-0379

February 2026| Volume 05 | Issue 01 | Pages 180-194

Journal homepage: https://fupubco.com/futech

https://doi.org/10.55670/fpll.futech.5.1.16

Future Publishing LLC

Article

AI-enabled toward zero-emission buildings and clean mobility: PV–BIPV and battery storage integration: a case study of Diyala, Iraq

Youssef Kassem[1,2,3,4]*, Hüseyin Çamur[1,3], Ali Saad Aldayyeni[1], Abdalla Hamada Abdelnaby Abdelnaby[4]

[1]Department of Mechanical Engineering, Engineering Faculty, Near East University, 99138 Nicosia (via Mersin 10, Turkey), Cyprus
[2]Energy, Environment, and Water Research Center, Near East University, 99138 Nicosia (via Mersin 10, Turkey), Cyprus
[3]Science, Technology, Engineering Education Application, and Research Center, Near East University, 99138 Nicosia (via Mersin 10, Turkey), Cyprus
[4]Department of Civil Engineering, Civil and Environmental Engineering Faculty, Near East University, 99138 Nicosia (via Mersin 10, Turkey), Cyprus

ARTICLE INFO

Article history:
Received 15 August 2025
Received in revised form
18 October 2025
Accepted 19 November 2025

Keywords:
Iraq, Techno-economic, Rooftop PV system, BIPV, CO_2 emissions, Electric vehicles

*Corresponding author
Email address:
youssef.kassem@neu.edu.tr
youssef.kassem1986@hotmail.com

DOI: 10.55670/fpll.futech.5.1.16

ABSTRACT

Iraqi buildings continue to rely heavily on fossil fuels, which raises carbon emissions and energy costs. To address this knowledge gap, the primary objective of the present study is to assess the techno-economic and environmental performance of solar energy retrofitting for a two-story mixed-use building in the eastern Iraqi province of Diyala, utilizing ERA5 reanalysis data for the first time. To this aim, three retrofit scenarios are considered ((1) the baseline scenario (BS) with no renewable systems, (2) the second scenario (SS) with a rooftop photovoltaic (PV) system, and (3) the third scenario (TS) combining rooftop PV, building-integrated photovoltaic (BIPV) glazing and a 30 mm layer of Expanded Polystyrene (EPS) insulation). The simulations were conducted with and without battery storage (103.2 kWh capacity) to demonstrate grid independence and energy self-sufficiency. The findings demonstrate that the TS scenario achieved net-zero or carbon-positive operation, as evidenced by the reduction of annual CO_2 emissions from 39,122 kg (BS) to –9,257 kg (TS), which represents net export of renewable energy to the grid. Economically, SPP ranged from 3.2 to 5.4 years without a battery and from 10 to 14 years with one, and LCOE ranged from 0.038 to 0.072 USD/kWh, demonstrating long-term viability. Furthermore, 90–120 electric vehicles might be charged each month using the extra daylight energy, encouraging sustainable mobility. This study shows that it is possible to create zero-emission buildings that use integrated PV and BIPV systems to allow EV charging, improve grid stability, and lower CO_2 emissions all at once. Besides, the innovative potential of integrated PV-BIPV-battery systems for zero-emission buildings to decarbonize Iraq's urban energy infrastructure is demonstrated in this study.

1. Introduction

Human activity is known to be the primary driver of climate change, particularly due to rising greenhouse gas emissions and environmental degradation [1]. The IPCC Climate Change Synthesis Report 2023 emphasizes the need for sustainable energy policies, noting that human activities, particularly unsustainable energy consumption, have elevated Earth's surface temperatures by 1.1°C relative to the pre-industrial levels [2]. According to the United Nations Climate Change [3], achieving these targets requires a 43% reduction in greenhouse gas emissions by 2030 and a peak in emissions by 2025. The Sustainable Development Goals (SDGs) [4] emphasize the significance of renewable energy in reducing global warming. One essential sustainable energy source is solar energy. Unlike fossil fuels, solar energy harnesses sunlight, an abundant and inexhaustible natural

resource, converting it into electricity with minimal environmental impact [5]. The demand for solar photovoltaic (PV) systems is rising rapidly among renewable energy sources due to several factors, such as declining costs and high returns on investment [6]. Recently, rooftop solar photovoltaic (PV) systems have gained prominence as a powerful decentralized energy solution [7]. According to Poornima et al. [8], these systems can help minimize land-use conflicts, reduce transmission losses, and enable businesses and homes to generate their own electricity.

Besides, PV technologies can be integrated into building envelopes as Building-Integrated Photovoltaics (BIPV) and have been considered a sustainable design solution for a built environment that is green and clean [9, 10]. Unlike conventional rooftop PV systems, BIPV technologies serve two functions: they act as building materials that can replace façades, skylights, windows, shading devices, and roofing elements while generating renewable electricity [11-13]. Additionally, BIPV offers significant aesthetic advantages, as photovoltaic components can be customized to meet architectural intent in terms of color, texture, transparency, and shape [11]. This ability facilitates a more natural integration of renewable technologies into dense urban environments, where cultural identity and visual coherence are crucial design factors [11, 14]. In addition to their aesthetic value, BIPV systems can generate electricity and replace conventional shading devices, providing a twofold advantage for energy-efficient design, as noted in Refs. [15, 16]. A bifacial BIPV façade renovation raised the annual percentage of hours in the thermal comfort range by around 8% in a real-world case study, according to Serrano-Lujan et al. [15]. Moreover, energy consumption can be significantly reduced without compromising architectural style when BIPV systems are used as double-skin envelopes in hot, dry locations. Additionally, buildings can become more valuable, have a smaller carbon footprint, and be certified LEED (Leadership in Energy and Environmental Design) when BIPV is used [17]. In addition to generating energy, BIPV systems can improve a building's acoustic and thermal insulation and provide other practical benefits. This dual use as a building material and an energy source represents a major advancement toward sustainable urban development [18, 19].

Iraq faces severe power shortages due to decades of insufficient planning, aging infrastructure, and rapidly rising demand, despite having the fifth-largest oil reserves in the world and significant natural gas resources [20, 21]. As a result, there have been regular power outages, forcing homes and businesses to use expensive residential generators at significant personal financial expense [21]. According to the World Bank Group (Global Solar Atlas), specific photovoltaic power generation ranges from 4.34 to 5.26 kWh/kWp. Hence, Iraq currently has significant potential to generate solar energy. Moreover, previous studies on solar power potential concluded that grid-connected and standalone PV systems can deliver reliable electricity, lower CO_2 emissions, and achieve economic viability compared to fossil fuels [22-25]. According to the authors' review, most previous studies in Iraq have focused on small-scale solar applications, such as agricultural irrigation and residential water heating. Also, a few studies have analyzed grid-connected or integrated systems for large-scale power generation. These studies have highlighted the potential of solar power to reduce CO_2 emissions and the electricity crisis. Consequently, the present study aims to assess the technical, environmental, and economic feasibility of battery storage, rooftop photovoltaic, and building-integrated photovoltaic systems in a mixed-use zero-emission building in the Diyala Governorate, Iraq. Besides, the current study aims to analyze the potential use of excess solar energy to charge electric vehicles, especially during daylight hours, thereby raising the possibility of sustainable transportation and energy independence. To this aim, three retrofit scenarios are compared in this paper: Baseline Scenario (BS) with no renewable systems, Second Scenario (SS) with rooftop photovoltaic systems, and the Third Scenario (TS), which integrates all aforementioned systems besides 30 mm thick Expanded Polystyrene (EPS) insulation and BIPV glazing. The expected results of this study can provide a practical, replicable framework to reduce Iraq's electricity deficit, enable clean energy generation in buildings, and encourage the use of electric vehicles.

2. Materials and methods

2.1 Study area

Figure 1 depicts the Diyala Governorate, located in eastern Iraq, northeast of Baghdad. This region, which is approximately 17,685 km^2 in size, is one of the most significant agricultural and habitation areas in Iraq, as it and its surrounding waters (River Diyala) provide water for cultivation and domestic use. The climate is characteristic of central and eastern Iraq; it is semi-arid to desert. Although winters are warm with mean temperatures between 8 and 15°C, summers are hot and dry, with many days reaching over 45°C in July and August. The annual rainfall ranges from 200 mm on the plain to 400 mm in the northeastern foothills, with most rainfall occurring between November and March and being highly seasonal. Furthermore, solar irradiation data show that the mean values of direct normal irradiation, Global horizontal irradiation, and Diffuse horizontal irradiation are 1835.3 kWh/m^2, 1944.3 kWh/m^2, and 778.8 kWh/m^2, respectively. The area experiences an average air temperature of about 24.3°C, with terrain at 120 m above sea level, both of which affect the performance of PV systems. In general, agriculture and water supplies are hampered by unpredictable rains and frequent droughts. Summertime also often brings dust storms and prolonged dry spells, which worsen environmental and human health impacts. The Water Crisis. The governorate is experiencing a growing water crisis due to several interconnected factors. Diyala is mostly dependent on transboundary floods from Iran via the Diyala River and its tributaries. In Iran, upstream dam construction and diversion have severely reduced inflows, while climate change has made droughts more frequent and severe. Excessive groundwater pumping in the area raises salinity and lowers water levels, reducing soil fertility and agricultural output. It has a direct effect on the rural economy of the governorate, which has historically been associated with date, wheat, barley, and citrus production. Additionally, domestic urban water supplies often run out, exacerbating social and political conflicts. Moreover, Diyala faces a serious electricity crisis in addition to a water deficit. Diyala is not an exception to the ongoing underperformance of Iraq's national grid. Power outages are common, lasting several hours each day and impacting homes, businesses, and critical services. Summertime and increased demand for electricity from cooling systems exacerbate the shortfall. Water and energy shortages are exacerbated by inadequate supplies of dependable electricity, which also make it difficult to run irrigation systems, water pumping stations, and other vital infrastructure. The majority of houses and businesses use expensive private diesel generators, which are harmful to the environment and not long-term viable. The region lies at the

heart of Iraq's broader water-energy-food nexus challenges due to Diyala's physical and climatic features, transboundary water dependencies, climate change impacts, and energy constraints.

Figure 1. Location map

2.2 Dataset

In this study, the global reanalysis, namely ECMWF's ERA5, is used. ERA5 is selected for its high spatial resolution and hourly temporal resolution, which are well-suited to capturing the local climate and topography of the Diyala region. ERA5 covers 1979 to the most recent 5 days, providing estimates of a large body of atmospheric, oceanic, and land climate data from many satellite and conventional instruments. The resolution in the horizontal grid is 0.25°, equal to about 31 km. ERA5 is correlated with uncertainty data for all variables at lower spatial and temporal resolutions [26]. The reliability of ERA5 reanalysis data for wind-resource assessment is discussed in Ref. [27]. ERA5 has also been extensively tested, compared with previous reanalyses and with measurements at local and regional scales [28]. ERA5 surpasses MERRA-2 in every feature that was tested; the correlations are higher, and MAE and RMSE are by an average of 20 % smaller than MERRA-2 [29]. Ramon et al. [30] reported that ERA5 surface winds showed the best agreement, correlating and replicating the variance better than a multi-reanalysis mean at 35.1 % of the validation stations and were better than four reanalysis datasets (ERA-Interim, JRA55, MERRA2, and the NCEP/NCAR R1). ERA5 depicted the mean wind speed more realistically, was better correlated on flat surfaces, and performed better than the MERRA-2 and COSMO-REA6 reanalyses [31]. Pronk et al. [32] determined that ERA5 performs better than the Wind Integration National Dataset (WIND) Toolkit Long-term Ensemble Dataset (WTK-LED) according to the centered root-mean-square error (cRMSE) and correlation coefficient for both the on-land and offshore scenarios under all atmospheric stability conditions. Further, ERA5 long-term winds were well consistent with in-situ altimeter measurements [33] and outperformed CFSR with a higher correlation coefficient and lower errors [34] and outperformed ERA-Interim by 20 % [35]. Further, ERA5 was the most reliable of the four reanalysis datasets considered (EMD-ERA, ERA5, CFSR2, and MERRA-2), with the highest correlation coefficient of 0.93 against in-situ LIDAR [36].

2.3 Case study description

This study investigates the energy performance of a two-story mixed-use building in Diyala, Iraq, with a gross floor area of approximately 600 m^2. This building is chosen as a representative typology of small- to medium-sized commercial buildings typical in the region, where energy consumption is highly dependent on climatic conditions, particularly hot, dry summers. The building's internal layout, occupancy time schedules, and internal load patterns were simulated in DesignBuilder, enabling a precise analysis of the building's thermal and energy performance across different retrofitting scenarios. The ground floor (see Figure 2) is primarily used as a supermarket, and the central Market Hall occupies most of the area. This space is intended to support basic retail functions, including product display, customer traffic, and cold storage. With extended operating hours and the use of high-intensity lighting and refrigeration machinery, the Market Hall experiences significant internal heat gains, which contribute to cooling loads, especially during summer. In addition to this central shopping area, there are three ancillary rooms: a manager's office, a storeroom, and a toilet facility. Each of these spaces was considered as an independent thermal zone during simulation to allow for variation in occupancy, equipment use, and internal heat generation. Internal partitions between zones were simulated using appropriate thermal properties to allow a realistic assessment of inter-zone heat transfer. All spaces on the ground floor are served by a centralized HVAC system designed to provide thermal comfort for the various functional spaces. Moreover, the first floor (Figure 2) is arranged as a residential area, with the best design for a household's normal occupancy. It has three bedrooms (Bedroom 1, Bedroom 2, and Bedroom 3), three bathrooms, a central living area, and an independent laundry room. The living room, the main common space, occupies the largest area and is used for prolonged periods beyond working hours. Each bedroom was modeled as an independent thermal zone to allow for varying occupancy schedules and internal gain profiles. Bathrooms and the laundry room were also defined as separate zones to account for their specific thermal and ventilation characteristics. Natural ventilation is achieved through operable windows on multiple façades, and space conditioning is provided by independent split-type air conditioners in the main rooms. The loads of plugs and lighting were distributed according to housing-use patterns typical for occupant behavior in Mediterranean climate regions. Interior partitions were constructed using materials with thermal properties typical of real materials to provide accurate thermal zoning within the space. To compare the effects of different energy-efficiency and renewable-energy measures, three retrofitting scenarios are proposed as follows.

(a) The baseline scenario (BS) is the first one, where the building is simulated in its current condition with no envelope upgrading or renewable energy systems. The external walls are composed of two 10 mm-thick cement plaster layers, one on the inner side and one on the outer side, divided by a 200 mm concrete block. Windows are depicted using single-pane glazing, and there are no photovoltaics. This condition is used as a basis for comparison for analyzing the building's energy consumption in its original, unchanged form. In the scenario, the energy consumption profiles for winter, spring, summer, and autumn are illustrated in Figure 3. The results show that the highest demand is in the summer, especially during the 8:00 to 22:00 time interval when cooling loads dominate.

Winter and spring have relatively low and flat consumption, while autumn has an intermediate profile.

(b) In the second scenario (SS), glazing and wall construction of the window are not altered from the baseline. However, rooftop photovoltaic panels are introduced. The panels are mounted in five rows with 19 modules each, providing a total of 95 PV panels on the roof. This scenario allows assessment of the solar energy production impact on energy performance without altering any thermal property of the building. The results indicate that the hourly consumption patterns by season are identical to those for the baseline, as the thermal envelope and drivers for loads are unchanged. The results demonstrate that summer and autumn remain the peak demand seasons, though overall energy balance is improved as some of the demand is met by renewable electricity, as shown in Figure 3.

(c) The third scenario (TS) goes a step further from the second by incorporating other indicators of energy efficiency. In this case, building-integrated photovoltaic systems (BIPVs) are applied to all windows' glazing surfaces. These consist of glazing with photovoltaic cells incorporated into the exterior layer so that electricity can be generated on-site by the windows. Further, an insulating thermal layer is incorporated into the building envelope to further its capacity to resist heat transfer. This combined approach combines active renewable energy generation with passive envelope changes in order to optimize overall energy efficiency, reduce cooling loads, and reduce reliance on grid electricity. Generally, energy efficiency measures are integrated by combining building-integrated photovoltaics (BIPVs) with envelope insulation improvements (Figure 4).

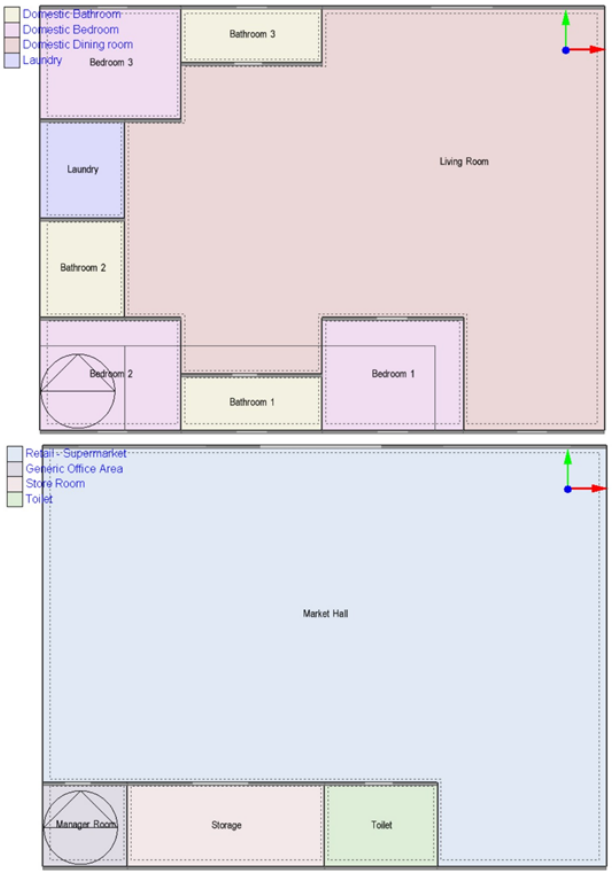

Zone Name	Space Area [m2]
GROUNDFLOOR:MARKETHALL	242.86
GROUNDFLOOR:MANAGERROOM	6.89
GROUNDFLOOR:STORAGE	17.72
GROUNDFLOOR:TOILET	9.84
FIRSTFLOOR:BATHROOM2	8.53
FIRSTFLOOR:BEDROOM2	16.77
FIRSTFLOOR:LIVINGROOM	186.94
FIRSTFLOOR:BATHROOM1	7.72
FIRSTFLOOR:BEDROOM1	17.22
FIRSTFLOOR:BEDROOM3	16.77
FIRSTFLOOR:LAUNDRY	8.53
FIRSTFLOOR:BATHROOM3	7.72

Scenario	Envelope Component	Reflectance	U-Factor with Film [W/m²·K]	U-Factor no Film [W/m²·K]	Total Gross Area [m²]	Total Net Area [m²]	Orientation
BS	External Walls GF	0.4	2.177	3.229	150.25	125.87	S/E/N/W
	External Walls FF	0.4	2.177	3.229	142.25	126.47	S/N/E/W
	Ground Floors	0.4	0.253	0.264	300	300	Horizontal
	Flat Roofs FF	0.15	0.25	0.259	259	259	Horizontal
	Windows / Glazing	-	1.8–3.0	-	-	-	N/S/E/W
SS	External Walls GF	0.4	2.177	3.229	150.25	125.87	S/E/N/W
	External Walls FF	0.4	2.177	3.229	142.25	126.47	S/N/E/W
	Ground Floors	0.4	0.253	0.264	300	300	Horizontal
	Flat Roofs FF	0.15	0.25	0.259	225	225	Horizontal
	Windows / Glazing	-	1.8–3.0	-	-	-	N/S/E/W
TS	External Walls GF	0.4	0.827	0.944	160.5	126.87	S/E/N/W
	External Walls FF	0.4	0.827	0.944	151	133.36	S/N/E/W
	Ground Floors	0.4	0.253	0.264	300	300	Horizontal
	Flat Roofs FF	0.15	0.25	0.259	259	259	Horizontal
	Windows / Glazing*	–	0.827–0.944 (improved)	–	–	–	N/S/E/W

* BIPV-integrated glazing for generating electricity; GF: Ground Floor; FF: First Floor; S: South; N: North; W: West; E: East

Figure 2. Description of the building

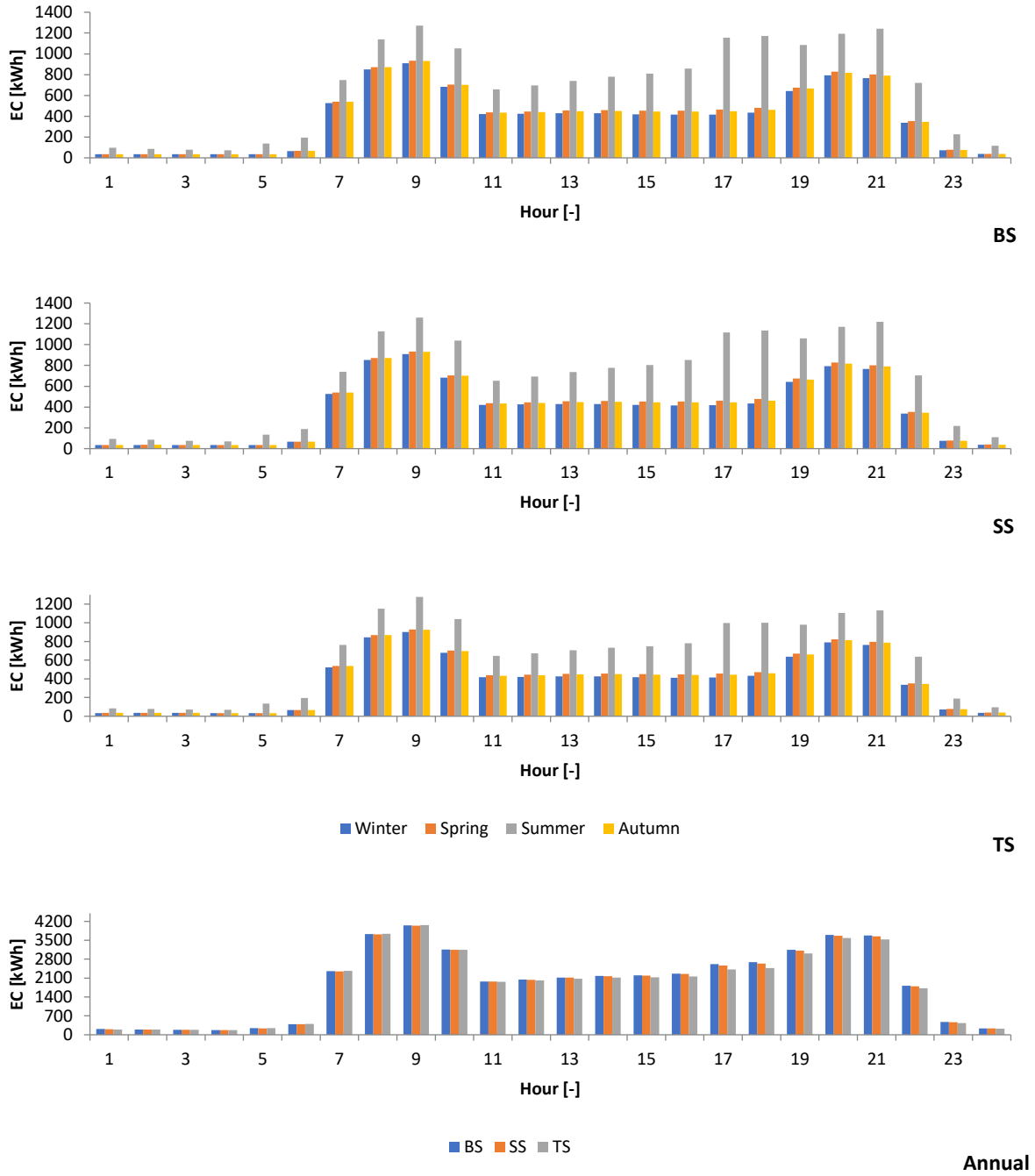

Figure 3. Energy consumption (EC) profiles for each scenario

2.4 Estimating the potential of solar power systems

Incident solar radiation on an inclined surface is a critical parameter in the design and performance assessment of solar energy systems. The tilted surfaces are oriented to capture the maximum possible solar radiation, based on the geographical location and seasonal solar path. It plays a significant role in the solar energy received, influencing the PV system's efficiency and energy yield. Thus, accurate estimation of solar radiation on tilted surfaces is crucial for the design of a solar power plant, as it depends on the optimal tilt angles. It is also crucial for determining an area's solar potential, enabling planners and engineers to estimate energy yields and ensure economic viability.

Moreover, the monthly output of the PV system can be calculated based on key factors such as the installed system capacity, the location's peak sun hours, and a derate factor that accounts for the combined effects of component efficiencies, system losses, and weather [38]. The amount of electricity to be generated by a photovoltaic system may be estimated on this basis. The mathematical equations for the energy output of an array of PV panels (E_{PV}) as a function of incident global solar irradiance (SR_i) are given below [38].

$$EG = \sum_{i=1}^{n} \eta_{PV} P_{STC} \left(\frac{SR_i}{G_{STC}}\right) \left[1 - \alpha_p (T_C - T_{STC})\right] N \Delta t_i \quad (1)$$

$$SR_i = G_b + G_d + G_r \quad (2)$$

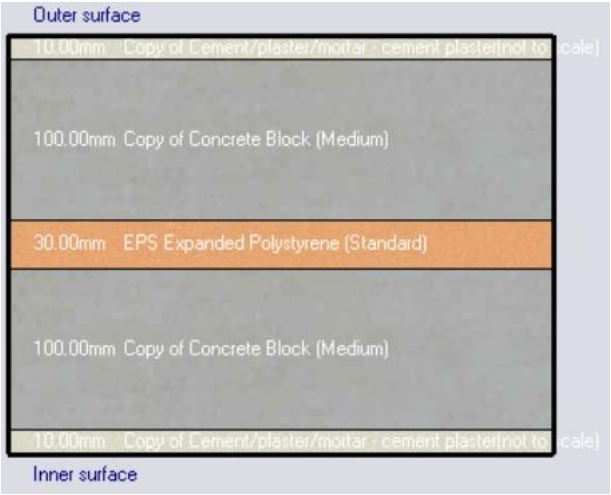

Figure 4. Building envelope insulation

For estimating the beam component from direct sunlight on the tilted surface (G_b) [38, 40, 41]:

$$G_b = \frac{G_{DH}}{cos\theta_z} cos\theta_i \quad (3)$$

$$cos\theta_z = sin\phi \cdot sin\delta + cos\phi \cdot cos\delta \cdot cos\omega$$

$$cos\theta_i = sin\delta \cdot sin\phi \cdot cos\beta - sin\delta \cdot cos\phi \cdot sin\beta \cdot cos\alpha + cos\delta \cdot cos\phi \cdot cos\beta \cdot cos\omega + cos\delta \cdot cos\phi \cdot sin\beta \cdot cos\alpha \cdot cos\omega + cos\delta \cdot sin\beta \cdot sin\alpha \cdot sin\omega \quad (4)$$

$$\omega = 15(12 - LAT) \quad (5)$$

$$LAT = standard\ tim\ (clock\ time) \pm 4(standard\ time\ longitude - longitude\ of\ location) + EOT \quad (6)$$

$$EOT = 229.18\big(0.000075 + 0.001868 \cdot cos(B) - 0.032077 \cdot sin(2 \cdot B) - 0.014615 \cdot cos(2 \cdot B) - 0.04089 \cdot sin(2 \cdot B)\big) \quad (7)$$

$$B = \frac{360 \cdot (N_d - 1)}{365} \quad (8)$$

For calculating the diffuse component (G_d) and reflected component (G_r) [38, 42, 43]

$$G_d = [GHI - G_{DN} cos\theta_i] \left(\frac{1+cos\beta}{2}\right) \quad (9)$$

$$G_r = \rho_{ground} GHI \left(\frac{1-cos\beta}{2}\right) \quad (10)$$

Where, δ: sollar declination angle, ϕ: Location's latitude, ω: Hour angle, β: Surface tilt angle concerning the horizontal plane, α: Surface azimuth angle, G_{DH} and G_{DN}: Direct horizontal solar irradiance and Direct Normal solar irradiance, respectively, GHI: Global horizontal solar irradiance, η_{PV}: Individual PV module derating factor (η_{PV} = 0.85), PSTC: Nominal power of an individual PV module, G: Plane-of-array irradiance, G_{STC}: Reference plane of-array irradiance under STC = 1 kW/m^2, ρ_{ground}: Ground reflectance (albedo), typically 0.1–0.3 (dimensionless), α_p: PV panel temperature coefficient of power, T_C: Operating cell temperature, T_{STC}: STC operating cell temperature = 25°C, N: Number of installed PV modules, N_d is the day of the year and Δt_i: Duration of the n time steps considered.

Additionally, one of the most important factors in determining the solar system's performance is the capacity factor. It is the ratio of the annual energy (E_{PV}) produced by the solar system to the annual maximum energy generation under optimal operating conditions. The expression for calculating it is shown in Eq. (11) [38].

$$CF = \frac{E_{PV}}{Installed\ Capacity \times 8760} \quad (11)$$

2.5 Estimating energy production from a BIPV system using PVGIS

The Photovoltaic Geographical Information System (PVGIS) is a web-based, free tool that aims to predict solar resources and the performance of PV systems in most countries worldwide [39]. PVGIS estimates monthly and yearly totals of electricity generation for various sun-tracking systems. PVGIS has implemented satellite-based meteorological databases, including the PVGIS climate monitoring satellite application facility (CMSAF), PVGIS-ERA5, PVGIS surface solar radiation dataset heliosat (SARAH), and PVGIS-COSMO. Solar radiation data for Europe, Asia, and Africa are obtained from the PVGIS-CMSAF and PVGIS-SARAH datasets; US data are obtained from the National Renewable Energy Laboratory (NREL) National Solar Radiation Database (NSRDB); and high-latitude region data are obtained from reanalysis products (PVGIS-COSMO and PVGIS-ERA5). In the current study, PVGIS 5 is used, and the PVGIS-ERA 5 dataset is used to simulate PVGIS 5. From satellite measurements, ERA5 provides global direct solar irradiation, the optimal angle for global irradiation, and average temperature.

2.6 Economic viability and carbon mitigation analysis

Evaluating the economic viability of renewable energy projects, such as solar energy systems, is essential to ensure financial sustainability and environmental stewardship. Simple Payback Period (SPP) and Levelized Cost of Energy (LCOE) are important metrics that are used in this evaluation. The SPP provides investors and policymakers with a clear indicator of risk and return by clearly defining the time it will take for the initial capital to be recovered, either as savings or revenues. Eq. (12) can be used to estimate the SPP value for the proposed system [44].

$$SPP = \frac{Investment\ cost}{Annual\ Saving} \quad (12)$$

The LCOE (Eq. 13) is a useful benchmark compared to traditional energy sources since it enables a thorough assessment of the unit cost of energy produced over the system's lifespan [38].

$$LCOE = \frac{SC_{lifteime}}{SEG_{lifteime}} \quad (13)$$

where $SC_{lifteime}$: Sum of cost over lifetime, and $SEG_{lifteime}$: Sum of electricity generated over the lifetime.

In addition to these cost-effective strategies, a carbon-reduction analysis is required to highlight the solar systems' positive environmental impacts, as they significantly lower greenhouse gas emissions compared to energy derived from fossil fuels. The carbon mitigation analysis can be estimated using the following equations [45].

$$CO_2 - MDS_{by} = AE_{PV} \times Ef \quad (14)$$

$$CO_2 - MDS_{from} = AE_{PV} \times CO_2 - MDS_{by} \quad (15)$$

$$NCO_2R = CO_2 - MDS_{by} - CO_2 - MDS_{from} \quad (16)$$

where $CO_2 - MDS_{by}$: CO_2 mitigation by a developed system, AE_{PV}: Annual energy generation, Ef: emission factor (0.7 kg/kWh), $CO_2 - MDS_{from}$: CO_2 mitigation from the developed system, NCO_2R: Net CO_2 reduction.

3. Results and discussion

3.1 Comparison of thermal behavior across building scenarios

Figure 5 shows the monthly variation of heating, cooling, and solar gains over the three building scenarios. The largest heating and cooling loads are shown in the reference scenario, suggesting that the building envelope, in its original configuration before any alterations, permits significant winter heat loss and significant summer solar heat gain. Besides, the energy consumption is slightly lower in the second scenario, where the wall structure and windows remain unmodified, but other minor modifications are implemented. This is particularly relevant for cooling loads during the summer. When BIPV glazing is used for all window orientations, the third scenario (TS) shows the most significant drop. Compared with the baseline, the zone and total sensible cooling loads are reduced by up to 15–20% during the summer months thanks to the BIPV glazing, which also significantly reduces solar heat transmission through the windows. Similarly, improved insulation qualities and less heat loss through window surfaces minimize the need for winter heating by about 20–25%. Additionally, solar gains over the windows drop by 20–30% as compared to the baseline method, especially during the hottest summer months. By preventing overheating in the summer and reducing heat loss in the winter, the TS configuration delivers superior overall thermal performance. This results in increased interior comfort, less annual energy consumption, and more potential for renewable energy generation through the integrated BIPV system. This outcome demonstrates that BIPV glazing can effectively maximize thermal and energy performance across all climatic seasons when used as part of an integrated, energy-efficient building envelope approach.

Moreover, the temperature profile shows the annual performance of interior and outdoor thermal conditions for the BS, SS, and TS scenarios, as shown in Figure 6. The outdoor dry-bulb temperature ranges from about -1°C in January to about 28°C in July, following a typical yearly pattern. The interior air, radiant, and operating temperatures are all directly impacted by this external variance, and all three exhibit similar yearly trends. Once more, the adoption of efficiency measures results in little but significant changes. Higher solar heat gain from the building enclosure is indicated by the baseline case (BS), which records the highest summertime radiant and room air temperatures. Although there are slight improvements in the second case (SS), the pattern remains identical because the glazing qualities remain the same.

Additionally, the third scenario (TS) demonstrates the maximum indoor thermal stability, using BIPV glazing to lower air, radiant, and operating temperatures by roughly 0.5 to 1°C during the hottest summer months. This shows that the window surfaces reduce heat gain, improving indoor comfort and lowering cooling loads. Interestingly, winter temperatures remain essentially unchanged, indicating that the BIPV glazing has no significant effect on passive solar heating. By reducing summer overheating without sacrificing pleasant winter conditions, the TS case more effectively achieves year-round thermal balance, increasing indoor thermal comfort and total building energy efficiency.

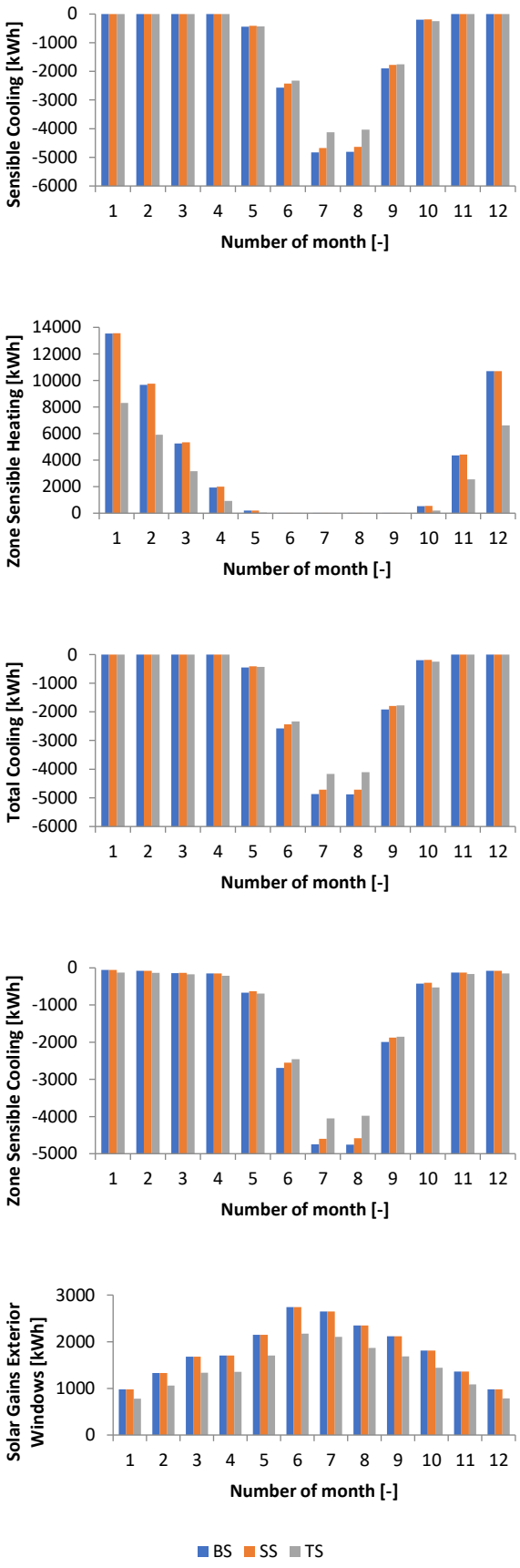

Figure 5. Monthly thermal Behavior for three building Scenarios

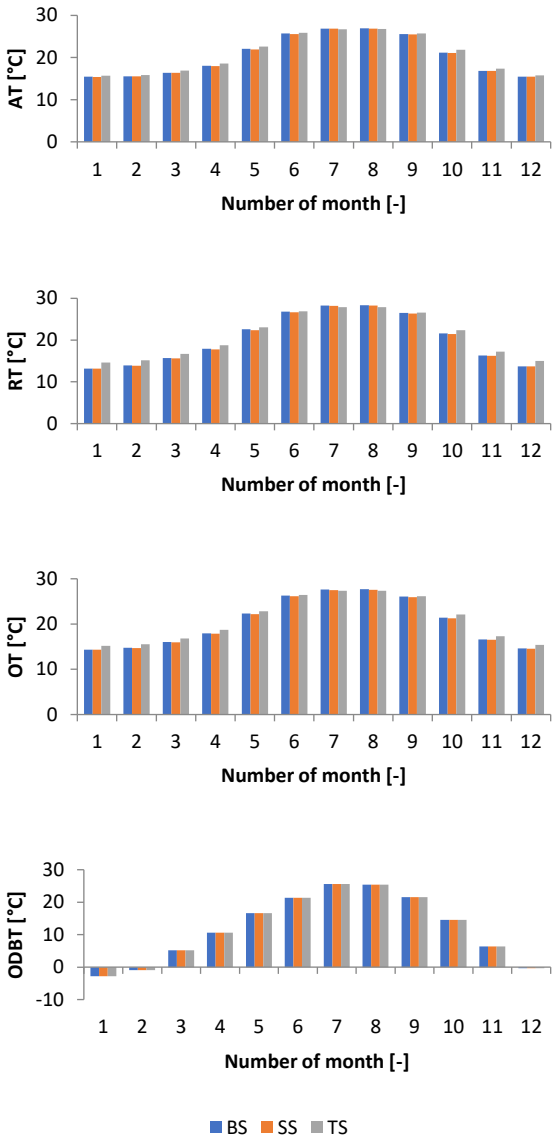

Figure 6. Monthly indoor and outdoor temperature behavior for three building Scenarios (AT: Air Temperature, RT: Radiant Temperature, OT: Operative Temperature, ODBT: Outside Dry-Bulb Temperature)

3.2 Optimal orientation and slope angle for rooftop PV system

In general, there are several types of solar panels available on the market, and new models are always being released due to the rapid advancement of technology. For the proposed system, the Tiger Neo N-type JKM570N-72HL4-BDV monocrystalline solar panel was selected for the rooftop PV system due to its robust power output, durable design, and exceptional efficiency. The specifications of the selected solar panel can be found in Table 1. Besides, AS-B60 320W Bifacial was selected for the BIPV system, and the specifications of it are listed in Table 2. The association between tilt angle, orientation, and annual energy yield on north-, south-, east-, and west-facing surfaces is determined by the analysis of the 54 kW rooftop PV system as shown in Figure 7 and Table 3.

Table 1. Specification of the selected solar panel (JKM570N-72HL4-BDV) at STC

Specification	Value
Maximum Power (Pmax)	570Wp
Maximum Power Voltage (Vmp)	42.29V
Maximum Power Current (Imp)	13.48A
Open-circuit Voltage (Voc)	51.07V
Short-circuit Current (Isc)	14.25A
Module Efficiency STC	22.07%
Operating Temperature	-40℃~+85℃
Nominal operating cell temperature	45±2℃
Temperature coefficients of Isc	0.046%/℃
Temperature coefficients of Voc	-0.25%/℃
Temperature coefficients of Pmax	-0.30%/℃

Table 2. Specification of the selected solar panel (AS-B60 320W Bifacial) at STC

Specification	Value
Maximum Power (Pmax)	320 Wp
Maximum Power Voltage (Vmp)	36.5 V
Maximum Power Current (Imp)	8.8 A
Open-circuit Voltage (Voc)	44 V
Short-circuit Current (Isc)	9.34 A
Module Efficiency STC	19.4%
Operating Temperature	-40 - 85 °C
Temperature coefficients of Pmax	0.41 %/°C

For all tilt angles, the south-facing orientation yields the most PV energy output of any arrangement, confirming its ability to maximize solar energy extraction in the research area. According to the findings, the north-facing panels' ideal slope angle is around 30°, at which the PV energy yield peaks at about 96,000 kWh/year, in line with the observed peak capacity factor (CF). The output gradually decreases as the slope exceeds 30° because the panels receive less direct sunlight throughout the summer. However, in winter, when there is less sun incidence, shallower angles (less than 20°) also result in poorer efficiency. Due to their limited exposure to direct sunlight, the north-facing panels produce the least amount of energy, with production steadily decreasing as the slope angle increases. At lower tilt angles (10° to 20°), which capture more morning or afternoon sun, respectively, the east- and west-facing orientations perform mediocrely, with slightly higher generation. However, they drastically decline after 30°. In conclusion, the findings demonstrated that a north orientation with a tilt angle of 30° is the best compromise between system efficiency and annual solar radiation harvesting, aligning with the location's solar geometry and optimizing the potential energy yield.

3.3 Monthly energy balance and contribution from PV systems

The monthly energy data shown in Table 4 reveal trends in grid dependency and PV generation across the BS, SS, and TS scenarios. Due to high cooling loads, grid energy consumption varies seasonally, peaking in the summer (June to August) and falling in the spring and autumn months. As mentioned before and shown in Table 4, the BS consistently exhibits the highest rate of grid power dependence, while the SS shows a fractional decrease in grid energy demand due to minor efficiency gains.

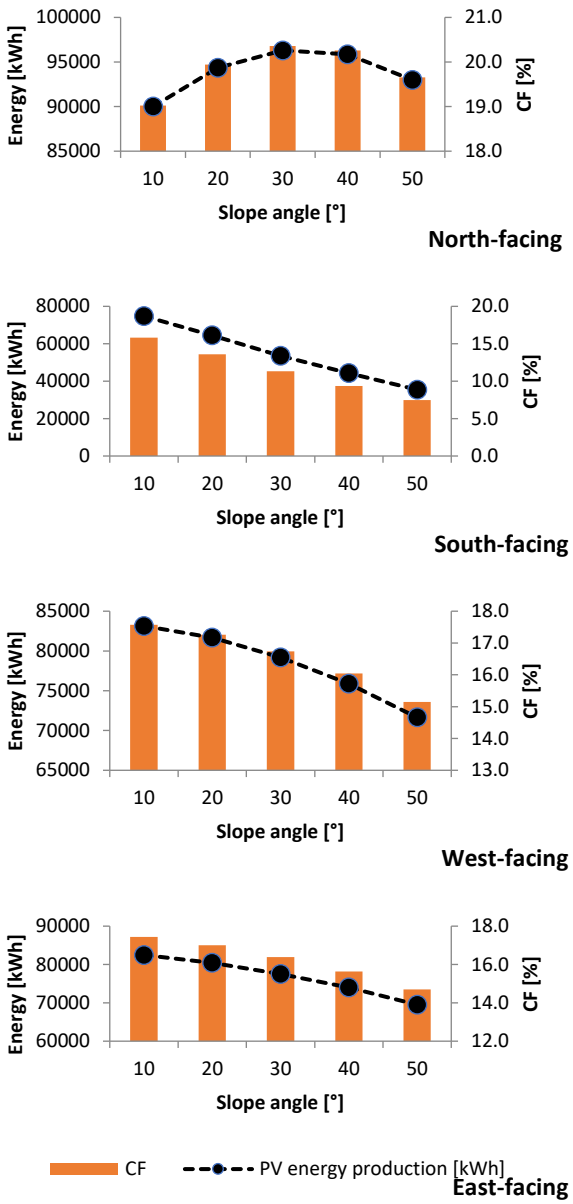

Figure 7. Annual value of energy production from a rooftop PV system and capacity factor with various orientation angles

Table 3. Monthly variation of energy demand and production

Variable	Slop angle [°]	Orientation azimuth angles [°]			
		North-facing	South-facing	East-facing	West-facing
PV energy production [kWh]	10	90003	74785	82470	83140
	20	94340	64388	80432	81668
	30	96303	53553	77538	79174
	40	95845	44270	73959	75896
	50	92980	35452	69503	71643
CF [%]	10	19.03	15.81	17.43	17.58
	20	19.94	13.61	17.00	17.26
	30	20.36	11.32	16.39	16.74
	40	20.26	9.36	15.63	16.04
	50	19.66	7.49	14.69	15.15

Table 4. Monthly variation of energy demand and production

Month	Energy from the grid			Energy production from PV		
	BS	SS	TS	Rooftop	BIPV	Total
Jan	3219	3219	3196	7024	1220	8244
Feb	2883	2883	2862	7188	1238	8426
Mar	3218	3218	3195	8605	1464	10069
Apr	3044	3044	3023	8520	1433	9953
May	3467	3447	3437	8721	1451	10172
Jun	4539	4460	4378	8303	1376	9679
Jul	5861	5775	5446	8539	1408	9947
Aug	5931	5837	5475	8977	1473	10451
Sep	4108	4039	4005	8686	1434	10119
Oct	3330	3321	3334	8064	1350	9414
Nov	3107	3107	3085	7016	1198	8214
Dec	3155	3155	3133	6800	1177	7977

Besides, TS exhibits the lowest grid energy consumption and evaluates the effectiveness of combined renewable energy installations in reducing electricity consumption. As shown in Table 4, the rooftop PV system provides the maximum monthly energy during March-August, ranging from approximately 8,300 to 8,900 kWh (Figure 8), while the BIPV system adds 1,200–1,470 kWh per month, depending on solar irradiance conditions. The combined PV generation is highest in August (10,451 kWh) and is always more than 9,000 kWh from March to September. However, due to lower solar radiation, generation is at its lowest in December (7,977 kWh) and January (8,244 kWh). In the TS scenario, where total PV generation meets the majority of building energy demand, the combined rooftop and BIPV system contribution significantly reduces grid dependence each month. These findings clearly show that combining BIPV with traditional rooftop PV expands building energy independence, optimizes overall renewable energy production, and permits a reduction in annual grid electricity demand and related greenhouse gas emissions. The integration of rooftop PV and BIPV systems in the TS scenario not only reduces reliance on the grid but also yields substantial energy savings throughout the year. The surplus generated energy (Figure 9), particularly during months with high solar radiation such as April to September, can exceed the building's operating demand, thus providing potential for secondary uses such as charging electric vehicles (EVs).

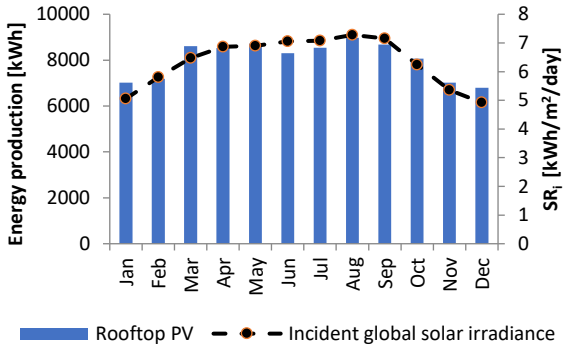

Figure 8. Monthly variation of surplus generating energy (SRi: Incident global solar irradiance)

Based on monthly generation, PV systems generate 9,500–10,000 kWh/month, and the building's grid energy requirement under the TS configuration decreases significantly compared to the baseline. This indicates that a portion of the renewable electricity can be directed toward charging electric vehicles, supporting sustainable transport initiatives without increasing the overall energy profile. Additionally, in this investigation, a lithium-ion battery storage system with a total capacity of 103.2 kWh was used to store extra energy generated by the PV system during the day. The technical specifications of the battery module are shown in Table 5. In this study, it is assumed a depth of discharge (DoD) of 80%, a round-trip efficiency of 90%, and a hybrid inverter efficiency of 99.9%. It should be noted that the hybrid inverter (XG50KTRL) with a power rating of 80kW is used in this study. The number of batteries used at night and for energy storage for the selected construction is displayed in Figure 10. The results show that a maximum of 35 batteries is required for the BS and SS, and 32 for the TS. BIPVs and energy-saving techniques can effectively reduce nighttime energy dependence and enhance system performance, as evidenced by the TS example, which reduced the number of batteries required.

3.4 Results of estimating the number of EVs and chargers

The most available electric vehicles (EVs) in Iraq are theCar#1: Tesla Model 3 (60 kWh), Car#2: Jaguar I-PACE (92 kWh), Car#3: Tesla Model S (100 kWh), Car#4: BYD DOLPHIN (44 kWh), Car#5: MG ZS EV (72.6% kWh), and Car#6: HYUNDAI KONA ELECTRIC (64 kWh). A 22 kW commercial/public charger was employed in this investigation. Figure 11 displays the number of EVs that are charged by the surplus energy generated during the daytime period for six different car models (Car#1–Car#6) for the three scenarios.

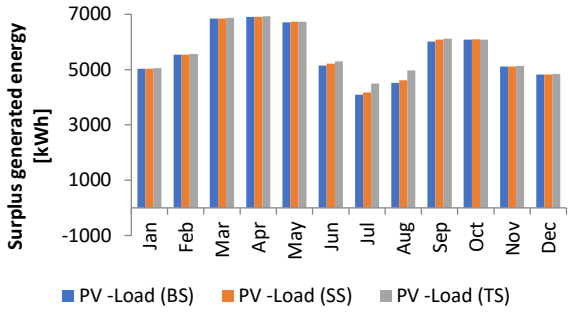

Figure 9. Monthly variation of surplus-generating energy

Table 5: Specification of Lithium Battery

Specification	Value
Cell type	LFP48173170E-120Ah
Module type	HJESLFP-38240
Combination	(192S~240S) 2P
Nominal Voltage (V)	614.4~768
Nominal capacity (Ah)	240
Nominal energy (kWh)	147.46~184.32
Standard charge current (A)	120 (0.5)
Maximum charge current (A)	150 (0.625C)@5S
Standard discharge current (A)	120 (0.5)
Maximum discharge current (A)	150 (0.625C) @5S
Operating voltage (V)	500~850

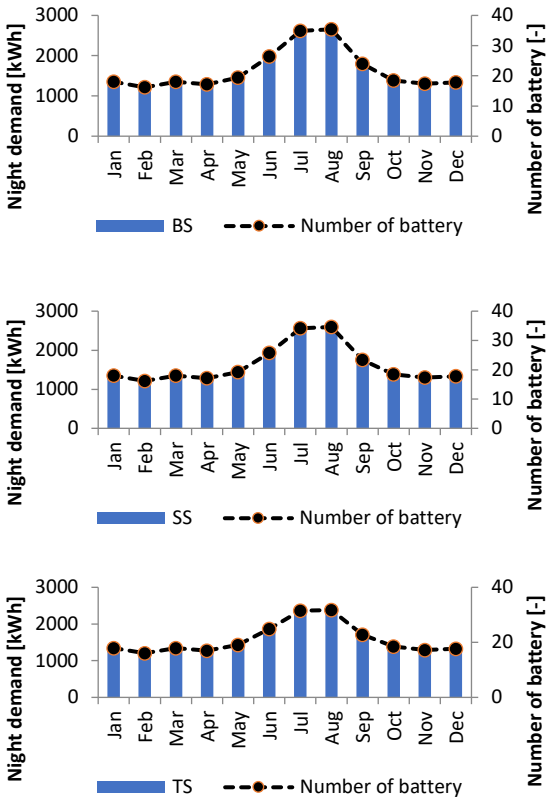

Figure 10. Monthly variation of energy demand at night and the number of batteries

The results indicate that the TS case consistently yields the highest number of EVs charged across all months and car types, followed by the SS and BS cases. This improvement in the TS scenario results from the addition of BIPV systems, which significantly increase overall energy generation and reduce building energy consumption, yielding more surplus energy for EV charging. Seasonally, the maximum EVs that can be charged are in the spring and early summer months (March–May), which coincide with more solar radiation and more PV system production. June and July have the lowest number of charged EVs, primarily due to higher cooling demand and reduced excess energy available for charging. Of all car types, Car#1 and Car#4 carry the highest charging potential, charging up to around 100–120 EVs per month, whereas Car#3 and Car#5 show fairly low values. Based on annual charging, the TS scenario shows the highest total count of EVs charged, followed by the SS and BS cases, which represent the overall energy efficiency gains achieved when incorporating BIPV.

These findings underscore the twofold benefits of PV systems: not only providing building energy needs but also facilitating clean transportation by supplying renewable electricity to charge electric vehicles during the daytime.

the seven public chargers is USD 3,000 apiece, for a total of

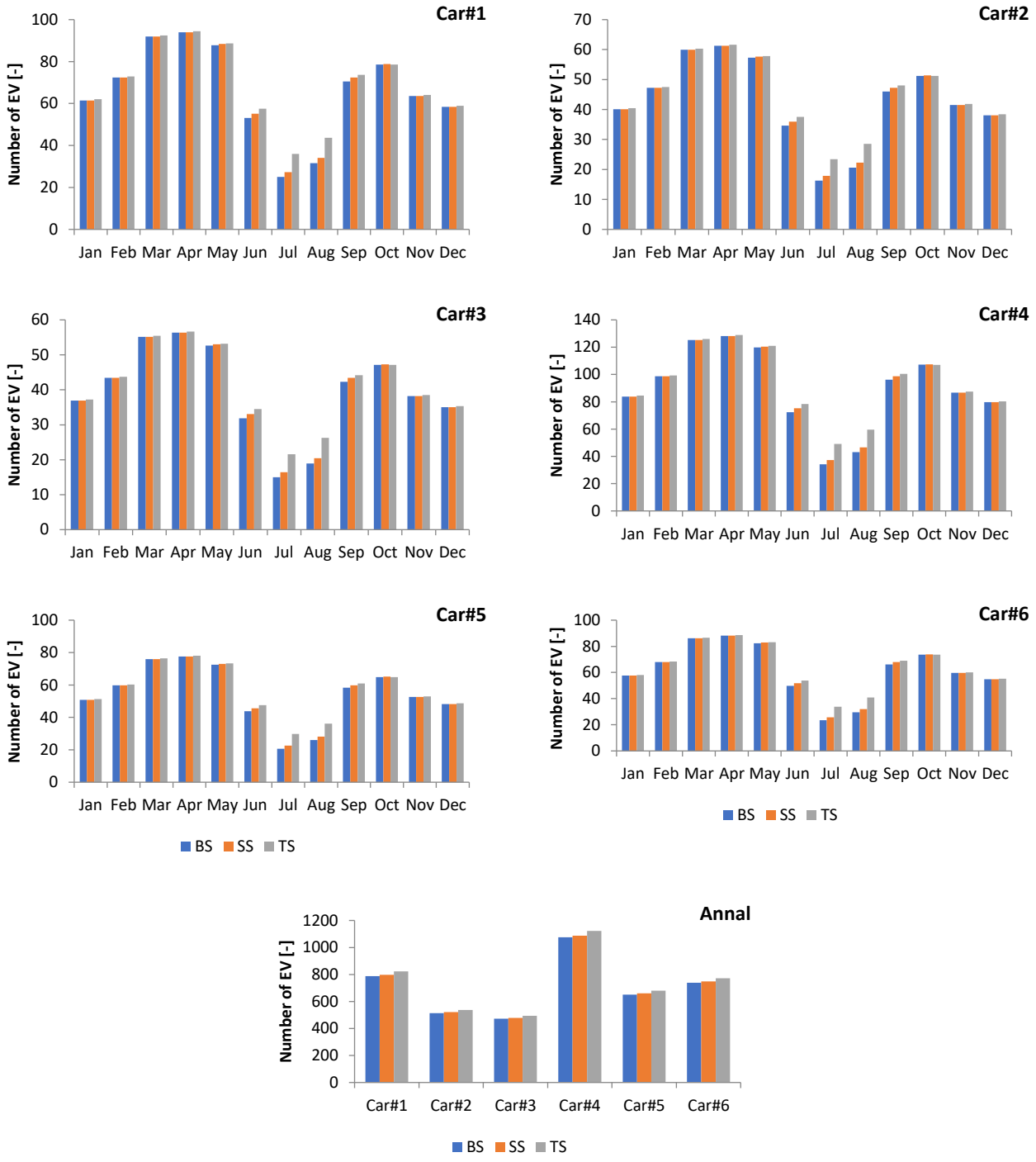

Figure 11. The number of electric vehicles that are charged by the surplus energy generated during the daytime period

3.5 Results of economic viability

Based on prior research and literature on Iraq, some assumptions have been made to evaluate economic viability. The proposed system's initial investment, with and without a battery, is USD 53652 and USD 466548, respectively. Note that, according to the TS case, there are 32 batteries. This includes 31 solar panels (AS-B60 320W Bifacial) at USD 75 each and 95 PV panels (JKM570N-72HL4-BDV) at USD 91 each. The price of a hybrid inverter is USD 8,000. The cost of

The remaining expenses are 0.6% for engineering and feasibility, 8.6% for installation and spare parts, and 3% for contingencies. This carefully considered cost breakdown guarantees that all important expenses and levies are included in the project budget. According to local economic projections and other studies on investments in renewable energy, a 9% discount rate has been used for financial computations to account for the time value of money. In

accordance with regional economic patterns, a 3% inflation rate was also anticipated. Operational and maintenance (O&M) expenses were accounted for at a standard rate of 1.5% of the annual total cost of capital, which is typically used in feasibility studies for renewable energy worldwide.

Figure 12 shows the relationship between the electricity selling price (USD/kWh) and the Simple Payback Period (SPP) of the proposed PV system in two working conditions, with storage and without storage. The results indicate a strong negative correlation between the selling price and payback period in both conditions, with extremely high coefficients of determination (R^2 = 0.9731), which confirms an excellent model fit. The payback period for a system without battery storage is comparatively short, ranging from one to five years, depending on the electricity's selling price. This is mostly because there is no extra expense for purchasing and maintaining batteries, and the initial capital expenditure is relatively low. The system's sensitivity to market energy prices is demonstrated by the payback period increasing as the selling price of electricity declines. However, when the battery storage facility is taken into account, the payback period rises significantly to roughly 10 to 45 years. This is because the battery units and related energy management systems demand a larger initial investment. However, adding batteries improves long-term operational redundancy and energy autonomy, particularly for areas with intermittent grid supplies or time-of-use electricity prices. According to the research's findings, battery-integrated systems are more reliable and energy-independent over the long run, without battery systems offering more financial advantages in the short term. In order to make judgments for investors and policymakers when assessing PV projects with or without storage, the quadratic regression formulas shown in the figure can be used to estimate the payback period for different power selling prices.

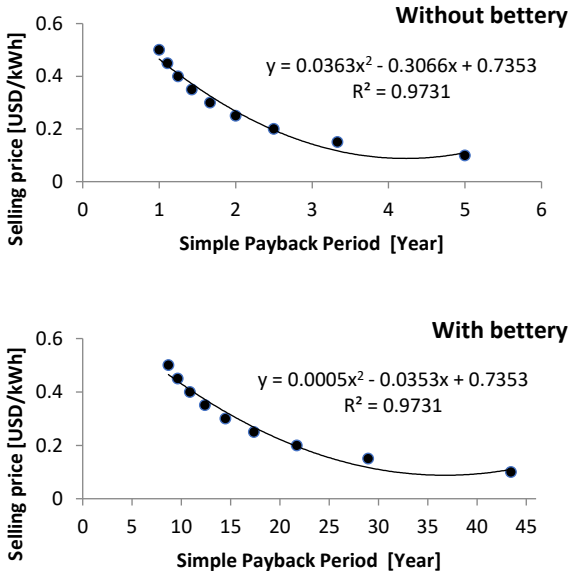

Figure 12. Relationship between electricity selling price and simple payback period

3.6 Results of Emission Reduction Analysis

The monthly variation in CO_2 emissions (kg) for the three scenarios under investigation is shown in Figure 13. The findings clearly show that combining energy-efficient procedures and BIPV systems can significantly reduce emissions. In BS, when no efficiency measures are performed, monthly CO_2 emissions range from around 2,148 to 5,159 kg, with higher values in January and July months when heating and cooling demand is greater. Emissions in SS drop dramatically, even going negative for every month but November and December (April to October), when improvements in building envelope and system efficiency are taken into account. This shows that the system produces extra clean energy to offset emissions from other sources in addition to meeting the building's energy requirements. The TS shows the most significant environmental positive impact when energy-saving measures and BIPV installations are implemented. Except for a few cold months (January, February, and December), CO_2 emissions are negative for practically the whole year. Net-zero or carbon-positive operation is represented by negative emission numbers, when the system generates more renewable energy than the building consumes, hence negating the need for fossil fuel-based grid electricity. June's lowest emission estimate, roughly -2,733 kg CO_2, indicates the system's greatest renewable generating capability when solar radiation is at its strongest. In the SS and TS scenarios, the building's PV system generated more renewable energy than the building's overall energy consumption, as indicated by the negative CO_2 emission values. In certain cases, the extra electricity produced by the BIPV or PV systems is fed back into the grid, effectively offsetting CO_2 emissions that would otherwise be attributed to fossil fuel-based grid-provided electricity generation.

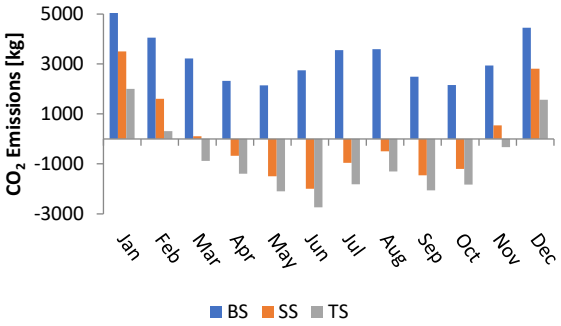

Figure 13. Monthly variation of CO_2 emission reduction

4. Discussion

The study's findings provide a comprehensive demonstration that rooftop PV-BIPV systems can significantly improve the technical, environmental, and financial performance of Iraq's building sector, particularly when integrated with enhanced thermal envelope measures. These findings are closely aligned with previous international and regional studies emphasizing the role of integrated renewable systems in achieving near-zero energy buildings (NZEBs) and ensuring sustainable energy transitions in developing countries. The findings indicated that the Third Scenario (TS), which includes rooftop PV, BIPV glazing, and EPS insulation, provides higher thermal performance and more energy savings. BIPV glazing successfully lowers solar heat gain in the summer and limits heat loss in the winter, as demonstrated by a 15–25% decrease in heating and cooling loads. Similar findings were found in previous studies [46-48]. These studies concluded that BIPV façades' low solar heat gain coefficient and accompanying energy generation can lower building cooling requirements by up to 20% in hot climate areas. Furthermore, in line with the improvements

shown in the TS scenario, Amani [49] and Lazaro et al. [50] demonstrated that installing EPS insulation in buildings can reduce energy consumption and improve thermal comfort. Moreover, it is found that systems without battery storage have a shorter return period (between 1 and 5 years) than systems integrated with batteries, which have a longer return period (between 10 and 45 years). These findings are supported by previous studies [51,52]. They revealed that storage solutions enhance system resilience and grid independence. However, in regions such as Iraq, which are susceptible to grid instability, integrating batteries provides long-term resilience and energy autonomy. The study also emphasizes the potential of excess solar energy in EV charging, which is an innovation. Furthermore, the TS scenario was able to achieve almost net-zero or even negative CO_2 emissions, with a maximum monthly decrease of about –2,733 kg CO_2. According to the International Energy Agency, solar systems can reduce about 0.38 kg CO_2 per kWh in areas dependent on fossil fuel-based power generation; this estimate is comparable with Iraq's energy mix. The current study concluded that Iraq's sustainability and decarbonization goals can be achieved by combining the environmental viability of PV and BIPV technologies with the significant emission reduction observed in this investigation.

5. Conclusion

This study examined the technical, environmental, and financial results of an integrated rooftop-BIPV solar system designed for residential use in Iraq. According to the findings, the proposed system significantly reduced greenhouse gas emissions and reliance on fossil fuels, thereby supporting Iraq's climate and sustainability objectives. In addition, the results demonstrated the potential for substantial energy cost savings and emissions reductions over the system's lifetime. Also, the study could contribute to enhancing energy security and supporting Iraq's transition to cleaner energy sources by integrating solar technologies into buildings' energy systems. The study emphasized how design parameters-tilt angle, orientation, and capacity-should be optimized in pursuit of maximum efficiency. Further areas of research should include long-term monitoring and sensitivity analyses regarding climate variability, dust accumulation, and fluctuations in energy demand. In general, these results will be helpful to policymakers, engineers, and households to promote the adoption of renewable energy and to further sustainable development in Iraq and other regions with high solar potential.

Ethical issue

The authors are aware of and comply with best practices in publication ethics, specifically regarding authorship (avoidance of guest authorship), dual submission, manipulation of figures, competing interests, and compliance with research ethics policies. The authors adhere to publication requirements that the submitted work is original and has not been published elsewhere.

Data availability statement

The manuscript contains all the data. However, more data will be available upon request from the authors.

Conflict of interest

The authors declare no potential conflict of interest.

References

[1] Razeghi, M., Saifoddin, A. A., Abdoos, M., Yousefi, H., Salaripoor, H., Gobnaki, M. R., ... & Gholizadeh, M. H. (2025). Evaluating the economic impact of solar energy on local industries in Semnan, Iran. Future Sustainability, 3(1), 49-58. https://doi.org/10.55670/fpll.fusus.3.1.5

[2] Calvin, K., Dasgupta, D., Krinner, G., Mukherji, A., Thorne, P. W., Trisos, C., Romero, J., Aldunce, P., Barrett, K., Blanco, G., Cheung, W. W., Connors, S., Denton, F., Diongue-Niang, A., Dodman, D., Garschagen, M., Geden, O., Hayward, B., Jones, C., . . . Ha, M. (2023). IPCC, 2023: Climate Change 2023: Synthesis Report. Contribution of Working Groups I, II, and III to the Sixth Assessment Report of the Intergovernmental Panel on Climate Change [Core Writing Team, H. Lee and J. Romero (eds.)]. IPCC, Geneva, Switzerland. https://doi.org/10.59327/ipcc/ar6-9789291691647

[3] United Nations Climate Change, 2024. The Paris Agreement. United Nations Climate Change. In: https://unfccc.int/process-and-meetings/the-paris-agreement

[4] Kyei, S. K., Boateng, H. K., & Frimpong, A. J. (2025). Renewable energy innovations: fulfilling SDG targets. Clean Energy, 9(2), 190-203. https://doi.org/10.1093/ce/zkae109

[5] Sene, D., Sarr, A., Sako, M. K., Ouattara, A., Ndiaye, M. F., & Sambou, V. (2024). Improved photovoltaic energy production under partial shading using an innovative MPPT controller based on the Flying Squirrel Search Optimization algorithm. Future Energy, 3(3), 33-48. https://doi.org/10.55670/fpll.fuen.3.3.4

[6] Mutumbi, U., Thondhlana, G., &Ruwanza, S. (2024). Adoption of residential rooftop solar PV systems in South Africa: A scoping review of barriers. Heliyon, 10(10). https://doi.org/10.1016/j.heliyon.2024.e30937

[7] Ebhota, W. S., & Tabakov, P. Y. (2025). Integrating rooftop PV system in low-cost building plan: A pathway to improving energy access and environmental sustainability. Energy and Buildings, 116020. https://doi.org/10.1016/j.enbuild.2025.116020

[8] Poornima, P. U., Dhineshkumar, K., Kumar, C. K., Sumana, S., Sundari, M. R., Sivaraman, P., ... & Rajaram, A. (2025). Optimising rooftop photovoltaic adoption in urban landscapes: A system dynamics approach for sustainable energy transitions. Biomedical Signal Processing and Control, 100, 107071. https://doi.org/10.1016/j.bspc.2024.107071

[9] Constantinou, S., Al-naemi, F., Alrashidi, H., Mallick, T., & Issa, W. (2024). A review on technological and urban sustainability perspectives of advanced building-integrated photovoltaics. Energy Science & Engineering, 12(3), 1265-1293. https://doi.org/10.1002/ese3.1639

[10] Wang, W., Yang, H., & Xiang, C. (2023). Green roofs and facades with integrated photovoltaic systems for zero energy eco-friendly building–A review.

Sustainable Energy Technologies and Assessments, 60, 103426. https://doi.org/10.1016/j.seta.2023.103426

[11] Batista, F., Guimarães, A. S., & Palmero-Marrero, A. I. (2025). Building Integrated Photovoltaics: a multi-level design review for optimized implementation. Renewable and Sustainable Energy Reviews, 220, 115837. https://doi.org/10.1016/j.rser.2025.115837

[12] Smith, A. R., Ghamari, M., Velusamy, S., & Sundaram, S. (2024). Thin-Film technologies for sustainable Building-Integrated photovoltaics. Energies, 17(24), 6363. ttps://doi.org/10.3390/en17246363

[13] Shi, S., & Zhu, N. (2023). Challenges and optimization of building-integrated photovoltaics (BIPV) windows: a review. Sustainability, 15(22), 15876. https://doi.org/10.3390/su152215876

[14] Pelle, M., Lucchi, E., Maturi, L., Astigarraga, A., & Causone, F. (2020). Coloured BIPV technologies: Methodological and experimental assessment for architecturally sensitive areas. Energies, 13(17), 4506. https://doi.org/10.3390/en13174506

[15] Serrano-Lujan, L., Toledo, C., Colmenar, J. M., Abad, J., & Urbina, A. (2022). Accurate thermal prediction model for building-integrated photovoltaics systems using guided artificial intelligence algorithms. Applied Energy, 315, 119015. https://doi.org/10.1016/j.apenergy.2022.119015

[16] Cheng, Y., Gao, M., Dong, J., Jia, J., Zhao, X., & Li, G. (2018). Investigation on the daylight and overall energy performance of semi-transparent photovoltaic facades in cold climatic regions of China. Applied Energy, 232, 517-526. https://doi.org/10.1016/j.apenergy.2018.10.006

[17] Chen, L., Baghoolizadeh, M., Basem, A., Ali, S. H., Ruhani, B., Sultan, A. J., ... & Alizadeh, A. A. (2024). A comprehensive review of a building-integrated photovoltaic system (BIPV). International Communications in Heat and Mass Transfer, 159, 108056. https://doi.org/10.1016/j.icheatmasstransfer.2024.108056

[18] Jelle, B. P., Breivik, C., & Røkenes, H. D. (2012). Building integrated photovoltaic products: A state-of-the-art review and future research opportunities. Solar Energy Materials and Solar Cells, 100, 69-96. https://doi.org/10.1016/j.solmat.2011.12.016

[19] Peng, C., Huang, Y., & Wu, Z. (2011). Building-integrated photovoltaics (BIPV) in architectural design in China. Energy and buildings, 43(12), 3592-3598.

[20] Al-Hamadani, S. (2020). Solar energy as a potential contributor to help bridge the gap between electricity supply and growing demand in Iraq: A review. Int J Adv Appl Sci ISSN, 2252(8814), 8814.

[21] Al-Wakeel, A. (2021). Local energy systems in Iraq: neighbourhood diesel generators and solar photovoltaic generation. In Microgrids and Local Energy Systems. IntechOpen. https://doi.org/10.5772/intechopen.95280

[22] Aziz, A. S., Tajuddin, M. F. N., Zidane, T. E. K., Su, C. L., Mas' ud, A. A., Alwazzan, M. J., & Alrubaie, A. J. K. (2022). Design and optimization of a grid-connected solar energy system: study in Iraq. Sustainability, 14(13), 8121. https://doi.org/10.3390/su14138121

[23] Alshamri, H., Cockerill, T., Tomlin, A. S., Al-Damook, M., & Al Qubeissi, M. (2024). On–off-Grid Optimal Hybrid Renewable Energy Systems for House Units in Iraq. Clean Technologies, 6(2), 602-624. https://doi.org/10.3390/cleantechnol6020032

[24] Al-Kayiem, H. H., & Mohammad, S. T. (2019). Potential of renewable energy resources with an emphasis on solar power in Iraq: An outlook. Resources, 8(1), 42. https://doi.org/10.3390/resources8010042

[25] Aziz, A. S., Tajuddin, M. F. N., Adzman, M. R., Mohammed, M. F., & Ramli, M. A. (2020). Feasibility analysis of grid-connected and islanded operation of a solar PV microgrid system: A case study of Iraq. Energy, 191, 116591. https://doi.org/10.1016/j.energy.2019.116591

[26] Hersbach, H., Bell, B., Berrisford, P., Hirahara, S., Horányi, A., Muñoz-Sabater, J., ... & Thépaut, J. N. (2020). The ERA5 global reanalysis. Quarterly journal of the royal meteorological society, 146(730), 1999-2049.

[27] Gualtieri, G. (2021). Reliability of ERA5 reanalysis data for wind resource assessment: A comparison against tall towers. Energies, 14(14), 4169. https://doi.org/10.3390/en14144169

[28] Masoud, A. A. (2024). Hybrid wind-solar energy potential modeling using ERA5 and solar irradiation data in google Earth Engine. Renewable energy, 232, 121042. https://doi.org/10.1016/j.renene.2024.121042

[29] Olauson, J. (2018). ERA5: The new champion of wind power modelling?. Renewable energy, 126, 322-331. https://doi.org/10.1016/j.renene.2018.03.056

[30] Ramon, J., Lledó, L., Torralba, V., Soret, A., & Doblas-Reyes, F. J. (2019). What global reanalysis best represents near-surface winds?. Quarterly Journal of the Royal Meteorological Society, 145(724), 3236-3251. https://doi.org/10.1002/qj.3616

[31] Brune, S., Keller, J. D., & Wahl, S. (2021). Evaluation of wind speed estimates in reanalyses for wind energy applications. Advances in Science and Research, 18, 115-126. https://doi.org/10.5194/asr-18-115-2021

[32] Pronk, V., Bodini, N., Optis, M., Lundquist, J. K., Moriarty, P., Draxl, C., ... & Young, E. (2022). Can reanalysis products outperform mesoscale numerical weather prediction models in modeling the wind resource in simple terrain?. Wind Energy Science, 7(2), 487-504. https://doi.org/10.5194/wes-7-487-2022

[33] Ozbahceci, B. O. (2020). Extreme value statistics of wind speed and wave height of the Marmara Sea based on combined radar altimeter data. Advances in Space Research, 66(10), 2302-2318. https://doi.org/10.1016/j.asr.2019.08.025

[34] Zed, A. A. A., Kansoh, R. M., Iskander, M. M., & Elkholy, M. (2022). Wind and wave climate southeastern of the Mediterranean Sea based on a high-resolution SWAN model. Dynamics of Atmospheres and Oceans,

99, 101311. https://doi.org/10.1016/j.dynatmoce.2022.101311
[35] Belmonte Rivas, M., & Stoffelen, A. (2019). Characterizing ERA-Interim and ERA5 surface wind biases using ASCAT. Ocean Science, 15(3), 831-852. https://doi.org/10.5194/os-15-831-2019
[36] Prasad, K. M., Nagababu, G., & Jani, H. K. (2023). Enhancing offshore wind resource assessment with LIDAR-validated reanalysis datasets: A case study in Gujarat, India. International Journal of Thermofluids, 18, 100320. https://doi.org/10.1016/j.ijft.2023.100320
[37] Kassem, Y., Gökçekuş, H., & Gökçekuş, R. (2024). Towards Sustainable Energy Solutions: Evaluating the Impact of Floating PV Systems in Reducing Water Evaporation and Enhancing Energy Production in Northern Cyprus. Energies, 17(21), 5300. https://doi.org/10.3390/en17215300
[38] Kassem, Y., Çamur, H., & Hussein, A. (2025). Harnessing wind and solar power for electric vehicle charging: a feasibility study at Ikas supermarket, Lefkosa, Northern Cyprus. Future Technology, 4(3), 204-215. https://doi.org/10.55670/fpll.futech.4.3.19
[39] Abdallah, R., Juaidi, A., Salameh, T., Jeguirim, M., Çamur, H., Kassem, Y., & Abdala, S. (2022). Estimation of solar irradiation and optimum tilt angles for south-facing surfaces in the United Arab Emirates: A case study using PVGIS and PVWatts. In Recent advances in renewable energy technologies (pp. 3-39). Academic Press.
[40] Shukla, K. N., Rangnekar, S., & Sudhakar, K. (2016). Mathematical modelling of solar radiation incident on tilted surface for photovoltaic application at Bhopal, MP, India. International Journal of Ambient Energy, 37(6), 579-588. https://doi.org/10.1080/01430750.2015.1023834
[41] Demain, C., Journée, M., & Bertrand, C. (2013). Evaluation of different models to estimate the global solar radiation on inclined surfaces. Renewable energy, 50, 710-721. https://doi.org/10.1016/j.renene.2012.07.031
[42] Tian, Z., Perers, B., Furbo, S., Fan, J., Deng, J., & Dragsted, J. (2018). A comprehensive approach for modelling horizontal diffuse radiation, direct normal irradiance and total tilted solar radiation based on global radiation under Danish climate conditions. Energies, 11(5), 1315. https://doi.org/10.3390/en11051315
[43] EME 810: Solar Resource Assessment and Economics. Retrieved from https://courses.ems.psu.edu/eme810/node/685?utm_source=chatgpt.com
[44] Adeyeye, K. A., Ijumba, N., & Colton, J. S. (2021). A techno-economic model for wind energy costs analysis for low wind speed areas. Processes, 9(8), 1463. https://doi.org/10.3390/pr9081463
[45] Manoj Kumar, N., Sudhakar, K., & Samykano, M. (2019). Techno-economic analysis of 1 MWp grid connected solar PV plant in Malaysia. International Journal of Ambient Energy, 40(4), 434-443. https://doi.org/10.1080/01430750.2017.1410226
[46] Zhou, L., Qi, F., & Yan, X. (2024). A review of research on the passive effect of building photovoltaic systems and analysis of influencing factors. Solar Energy, 278, 112766. https://doi.org/10.1016/j.solener.2024.112766
[47] Mohammad, A. K., Garrod, A., & Ghosh, A. (2023). Do Building Integrated Photovoltaic (BIPV) windows propose a promising solution for the transition toward zero energy buildings? A review. Journal of Building Engineering, 79, 107950. https://doi.org/10.1016/j.jobe.2023.107950
[48] Azami, A., & Sevinç, H. (2021). The energy performance of building integrated photovoltaics (BIPV) by determination of optimal building envelope. Building and environment, 199, 107856. https://doi.org/10.1016/j.buildenv.2021.107856
[49] Amani, N. (2025). Energy efficiency of residential buildings using thermal insulation of external walls and roof based on simulation analysis. Energy Storage and Saving, 4(1), 48-55. https://doi.org/10.1016/j.enss.2024.11.006
[50] Lazaro, S. A. M., Li, X., & Baba, V. F. (2025). Building Envelope Renovation for Energy Efficiency in Maputo, Mozambique: Expanded Polystyrene Insulation and Double-Glazed Windows. Environmental and Earth Sciences Proceedings, 34(1), 9. https://doi.org/10.3390/eesp2025034009
[51] Ahmed, M. M., Bawayan, H. M., Enany, M. A., Elymany, M. M., & Shaier, A. A. (2025). Modern advancements of energy storage systems integrated with hybrid renewable energy sources for water pumping application. Engineering Science and Technology, an International Journal, 62, 101967. https://doi.org/10.1016/j.jestch.2025.101967
[52] Aslam, M. U., Miah, M. S., Amin, B. R., Shah, R., & Amjady, N. (2025). Application of energy storage systems to enhance power system resilience: A critical review. Energies, 18(14), 3883.https://doi.org/10.3390/en18143883